CATION BINDING SITES ON THE PROJECTED STRUCTURE OF BACTERIORHODOPSIN

NANDINI V. KATRE, YOSHIAKI KIMURA, AND ROBERT M. STROUD
Department of Biochemistry and Biophysics, School of Medicine, University of California, San Francisco, California 94143

ABSTRACT Divalent cations are involved in the function of bacteriorhodopsin (bR) as a light-driven proton pump. If cations are removed from purple membranes they become blue. Divalent cations such as Ca^{2+} or Pb^{2+} or trivalent ions, can be stoichiometrically titrated back on to these deionized membranes. The color transitions as a function of ion concentration for Ca^{2+} or Pb^{2+} are precisely comparable and indicate that approximately three stoichiometric equivalents of cations are required to effect the color transition (Kimura et al., 1984). We found four main partially occupied binding sites for cations at a stoichiometric ratio of 3 Pb^{2+}/bR. We localized the binding sites for Pb^{2+} using x-ray diffraction of membranes reconstituted with 1, 2, and 3 equivalents of Pb^{2+} per bR. The site of highest affinity is located on helix 7. At 2 Pb^{2+}/bR, sites on helix 6 and between helix 2 and 3 are occupied. At 3 Pb^{2+}/bR a fourth site above helix 3 is occupied.

INTRODUCTION

Bacteriorhodopsin (bR) is a membrane protein found as purple patches in *Halobacterium halobium* (Stoeckenius and Bogomolni, 1982). The chromophore, retinal, is bound via a Schiff base to lysine 216 in bR (Bayley et al., 1981; Katre et al., 1981). It absorbs light energy and pumps protons vectorially through the purple membranes (PM). The chromophore is sensitive to its charged environment (Mathies and Stryer, 1976; Nakanishi et al., 1980). In the native purple membranes the chromophore absorbs at λ max = 570 nm. Removal of cations from PM results in a purple-blue transition. The blue species has a λ max at 608 nm (Kimura et al., 1984) or at 630 nm (Chang et al., 1985). Purple color can be regenerated from the blue membranes by addition of cations (Kimura et al., 1984; Chang et al., 1985). Blue membranes have an altered photocycle that affects the proton pumping ability (Mowery et al., 1979; Tsuji and Rosenheck, 1979; Chang et al., 1985).

The photocycle of bacteriorhodopsin seems to be directly influenced by interaction of cations with the membrane (Chang et al., 1985; Dupuis et al., 1985). This seems to imply a possible role for divalent cations, either in the energy transducing mechanism or in maintaining structural integrity. To investigate these possibilities further we sought to define the binding of cations, to determine whether or not they were at discrete sites, and to quantitate the effects of ion binding on the structure by x-ray diffraction. To make comparisons most directly between the partially deionized and native (or reconstituted) membranes, with the aim of identifying ion binding sites, and separating these from structural change in the membranes as a function of cation association, we present here the difference density maps calculated between Pb^{2+}-containing membranes, and membranes fully reconstituted with 3 Ca^{2+} per bR. A preliminary version of these results was presented at the International Symposium on Biomolecular Structure and Interactions (1984). The protein may change its conformation when deionized, thus our difference maps describe differences with respect to the 3-Ca^{2+} membrane, being closest to the physiologically relevant "native" structure. Chang et al. (1985) suggest that Ca^{2+} and Mg^{2+} may be the cations associated with PM in the native state. Acceptance of a site as being due to Pb^{2+} with a particular stoichiometry of Pb^{2+}-3 Ca^{2+} PM, rather than a consequence of structural change in the protein, is based on (*a*) satisfactory refinement of site occupancies; and (*b*) that double difference maps after refinement of each site separately should always reveal the other site(s). These criteria seem to be effective and indeed all of the Pb^{2+} sites present in the 1 Pb^{2+} and 2 Pb^{2+} derivatives are also present together (and are refineable) in the 3 Pb^{2+}-3 Ca^{2+} difference maps, where we presume that the ion substitution is the only difference in true overall electron density distribution. The final double difference maps after co-refinements of acceptable sites should therefore be peak free.

MATERIALS AND METHODS

Purple membranes (PM) were isolated from *Halobacterium halobium* strain ET1001 (Oesterhelt and Stoeckenius, 1974). Blue membranes were prepared as follows: PM in nanopure water were passed through a

Dr. Katre's present address is Cetus Corporation, 1400 53rd Street, Emeryville, CA 94608.

Dr. Kimura's present address is National Institute of Physiological Sciences, Myodaiji, Okazaki 444, Japan.

cation exchange resin (BioRad Cellex-P, Richmond, CA, hydrogen form). The resin was alternatively washed with 1N NaOH, 1N HCL, and water until the pH of the supernatant after the water wash was neutral. In all procedures described here, the water used was nanopure (Sybron/Barnstead resistivity 18 megaOhm-cm). Protein concentration of bacteriorhodopsin in purple membranes was assayed by absorbance at 570 nm, using the extinction coefficient for the light-adapted form of bR: ϵ_{570} = 63,000 cm^{-1} M^{-1}. Concentration of blue membranes was assayed by absorbance at 608 nm, using ϵ_{608} = 60,000 cm^{-1} M^{-1} (Kimura et al., 1984). Optical densities were measured on a Beckman (Fullerton, CA) DU spectrophotometer equipped with a Gilford digital detection system (Oberlin, OH). All centrifugations were carried out in a Sorvall SS-34 rotor, (Dupont Co., Wilmington, DE) at 18,000 rpm for 30 min. All membrane preparations were kept in clean plastic tubes or quartz cuvettes to avoid any contact with glass. Titrations of the blue membranes with cations were done using $CaCl_2$(10 mM) or $PbCl_2$ (10 mM). Protein concentrations used were the same as used by Kimura et al. (1984).

X-RAY DIFFRACTION

The x-ray camera (length 5.321 cm) used for diffraction was designed by Ross and Stroud (1977). The source was a rotating anode generator (Elliott GX-6; G.E.C. Avionic Ltd., England), run at 0.8 kW with a 1.0 × 0.1-mm focus. The beam was Ni-filtered and focused onto the film plane by double Franks' mirrors (Franks, 1955), with tantalum windows and passed through a 0.35-mm aperture before the specimen to diminish any parasitic scattering.

Samples for diffraction were prepared by pelleting Ca^{2+} reconstituted purple membranes and Pb^{2+} - containing membranes. Typically 2–4 pellets were subject to x-ray diffraction for each treatment of membranes. Membranes were pelleted on a Mylar (0.001 cm) window by centrifugation into specially designed polycarbonate sample holders contained in cellulose nitrate ultracentrifuge tubes. Centrifugation was in a Beckman SW-65 rotor at 50,000 rpm for 3 h at 5°C. Typically, the membrane pellets were ~0.5–1 mm thick. A small layer of water was allowed to remain above the pellet and excess water was removed by filter paper. The sample cell was sealed by another Mylar window. The membrane pellet was aligned with the membrane planes perpendicular to the focused x-ray beam. The sample was kept at 5°C and the camera between sample and film was purged with water-saturated helium. The diffraction pattern was recorded on Kodak "No Screen" or Reflex-25 x-ray film (CEA America Corp., Greenwich, CT). Patterns were digitized on a Syntex AD-1 microdensitometer, using a pixel size of 32 μm.

X-RAY DIFFRACTION

From the digitized patterns, the intensity profile was generated by radial integration and averaging. It is necessary to locate the center of the film to within ± 10 μm. The center was refined by integration over 20° sectors along the two axes of the diffraction pattern and comparison of the positions of pairs of equivalent reflections located on opposite sides of the film center. The optical density measurements were corrected for film nonlinearity using a logarithmic correction (Ross et al., 1977).

Raw intensity profiles were background-subtracted. A background curve was generated using a cubic spline fitting procedure of background points between reflections peaks. After background removal, the intensities of the overlapped reflections were separated by deconvolution of a Gaussian from the raw data, using an algorithm developed by Stroud and Agard (Agard et al., 1981). The incident x-ray wavelength is λ = 1.54178 Å for CuKα x-rays.

Intensities of the individual reflections were corrected by a Lorentz correction. The Lorentz correction accounts for the angular disorientations in the membrane pellets. We attempted to orient membranes by pelleting into a cell for x-ray diffraction. The x-ray beam was perpendicular to the membrane plane; parallel to the pelleting direction. Therefore, if the orientation were perfect, the Lorentz correction should be proportional $S = \text{Sin}\,\theta$, meaning intensity of each hk reflection is spread into a circle or circumference $2\pi S$. However, if misorientation of the planes is ±12° or more, the observed intensities sample an even lower section through these rings that spread perpendicularly to the membrane by a further factor of $S = \text{Sin}\,\theta$; the Lorentz factor is then $2\pi S^2$. To determine which value is most applicable, we derived n for the Lorentz factor $2\pi S^n$, which would make the x-ray intensities best match those from electron diffraction intensities of Hayward and Stroud (1981) for the zero level plane. The value of n was 1.8 (close to 2) implying that the misorientation of the membranes is about ±12° (see Appendix); therefore, we used the Lorentz correction $\sin^2\theta$ throughout.

The corrected peaks of intensity were integrated to obtain total intensity of each reflection. From the intensities (I_{hk}), the amplitudes ($F = \sqrt{I_{hk}}$) were calculated. For unobserved reflections, intensities used were one-half the smallest observable intensity. In cases where the intensities of the h, k and k, h reflections overlapped, their amplitudes were calculated by using the ratio of $F_{h,k}$ to $F_{k,h}$ obtained from electron diffraction of native PM (Hayward and Stroud, 1981).

The amplitudes from different films, or from different samples, were scaled to one another by a nonlinear least-squares procedure in which each reflection was weighted by $1/\sigma^2$, where $\sigma = \sqrt{F}$, $\sigma = \sqrt{2}$ for $|F| > 2$. Three Ca^{2+} reconstituted PM patterns were scaled to each other in a master set of native amplitudes (F_R). Data from each film within a derivative set of amplitudes (F_{Pb}) were first scaled to this master set, and then the scaled data for several films were averaged together.

Difference Fourier maps were computed using difference amplitudes ($\Delta F = ||F_{Pb}| - |F_R||$) and phase angles of native PM obtained by Hayward and Stroud (1981) using electron microscopy. Difference maps were also calculated between different subsets of native films or between subsets of derivative films to obtain the level of noise. Subsets of derivative and native data were used to calculate subset Fourier difference maps to examine consistency of the density features.

RESULTS

Titration curves of the blue-to-purple transition, as a function of Ca^{2+} and Pb^{2+} concentration were identical to one another (Kimura et al., 1984). These curves show that there are 2–3 tightly associated divalent cations per bR, up to the stage where the color change occurs.

The Ca^{2+} reconstituted patterns, treated as the "native," for comparison with Pb^{2+} membranes, were deionized and then reconstituted with Ca^{2+} to give the x-ray observed amplitudes $F_{R(hk)}$; the derivatives were reconstituted with stoichiometries of 1 Pb^{2+}, 2 Pb^{2+} or 3 Pb^{2+} per bR. At stoichiometries of 2 Pb^{2+} ions, or 1 Pb^{2+} ion per bR, the membranes are partially blue and the color change occurs after the range from 0 to 3 Pb^{2+}. We ultimately identified four discrete cation sites in the difference maps, indicating that several of the sites could be involved in the absorbance change, and that the fourth site may not be reflected in the absorbance change.

The background-corrected intensity profile of PM reconstituted with 3 Ca^{2+} is shown in Fig. 1 *a*. Similar profiles were obtained for all x-ray patterns. Fig. 1 *b* shows the pattern from the reconstituted PM after deconvolution

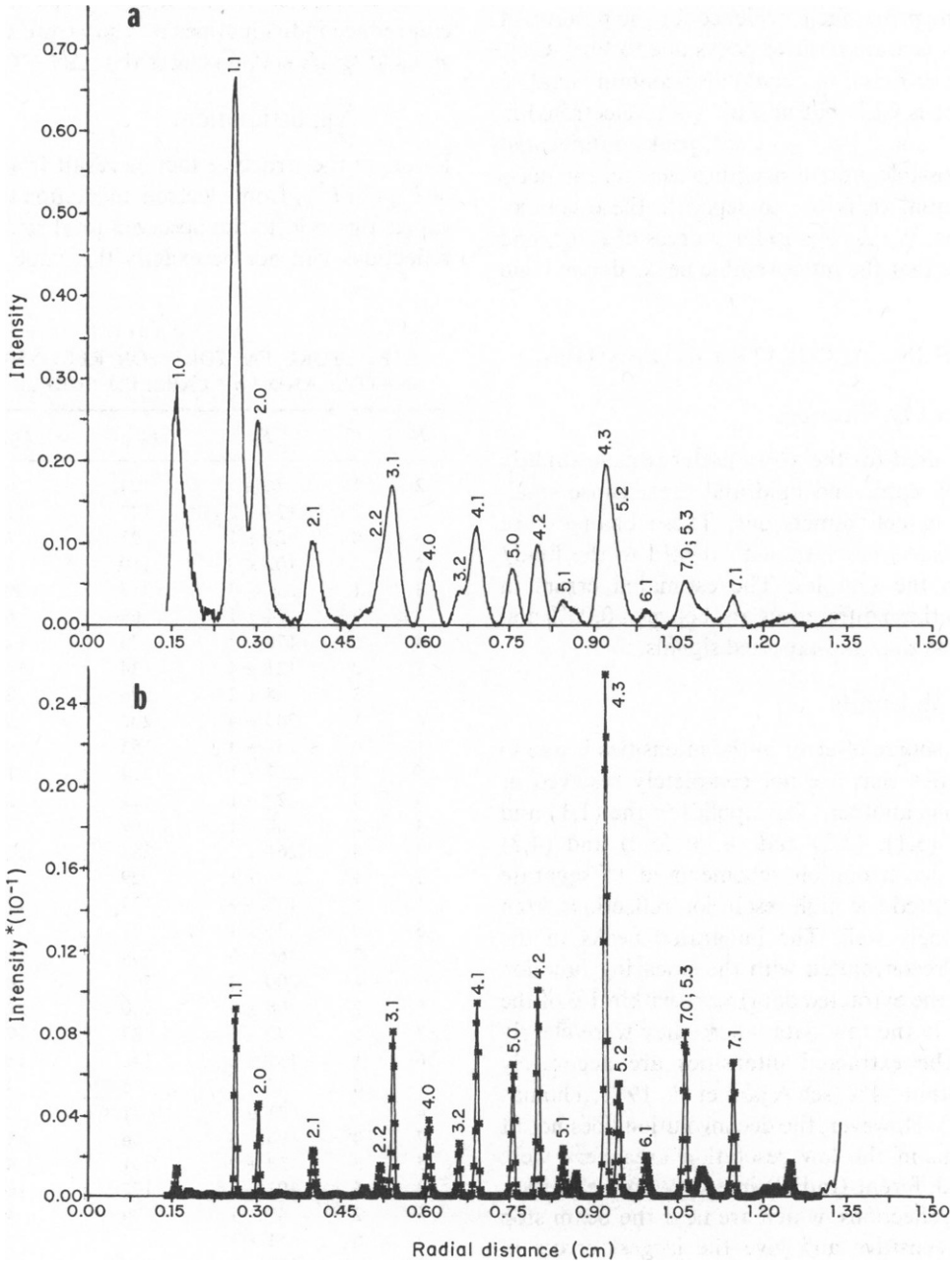

FIGURE 1 (*a*) Background-corrected x-ray intensity profile of PM reconstituted with 10 mM $CaCl_2$. Similar profiles were obtained for blue membranes titrated with 1 Pb^{2+}, 2 Pb^{2+}, or 3 Pb^{2+} per bR, using 10 mM stock $PbCl_2$. (*b*) Pattern in *a* after separation of overlapped reflections by deconvolution (Agard et al., 1981) and corrected by a Lorentz correction of $\sin^2\theta$.

of the broadening function and separation of the overlapped peaks. Table I lists the structure factors of reconstituted (F_R) and Pb^{2+} containing derivative (F_{Pb}) sets, calculated from the observed intensities of the reflections. When the h, k and k, h reflections overlap (i.e., for $h \neq k$, $h, \neq 0$, $k \neq 0$), structure factors were derived so as to preserve the ratios of $F^2_{h,k}$ to $F^2_{k,h}$ obtained from electron diffraction data of Hayward and Stroud (1981), where I_{hk} (observed) $= F^2_{h,k} + F^2_{k,h}$.

Difference Fourier maps between 1 Pb^{2+}, 2 Pb^{2+}, or 3 Pb^{2+} and the 3 Ca^{2+} reconstituted membrane are shown in Figs. 2 *a–c*, respectively. These images demonstrate that bound cations occupy discrete sites on the membranes. Such maps are the prima facie evidence for the position of sites. These maps contain positive peaks due to Pb^{2+}-Ca^{2+} (82 − 20 = 62 electrons), but could also contain negative peaks where there is Ca^{2+} but no Pb^{2+} (−20 electrons) in the case of 1 Pb^{2+} and 2 Pb^{2+} - 3 Ca^{2+}, peaks positive and negative due to possible protein structure change, and noise peaks. It is essential therefore to separate these components of the maps. We first consider sources of error, and then demonstrate that the interpretable peaks derive from bound cations.

ERRORS IN CALCULATED INTENSITIES

Chemical Differences

Pelleted samples used for the x-ray patterns have slightly different ratios of water and lipid and these cause small changes (<1%) in cell dimensions. These changes are random rather than systematic with regard to the lipid/water content in the samples. The estimated errors in intensities due to these differences are between 0.05% and 2% of $|F_R|^2$, far less than the expected signals.

Resolving Limits

Another possible source of error in the intensities is due to reflection intensities that are not completely resolved or separated from one another. This applies to the (1,1) and (2,0); (2,2) and (3,1); (3,2) and (4,1); (5,2) and (4,3) reflections. The deconvolution scheme used to separate these reflections fitted the high resolution reflections from 4,3 to 7,1 extremely well. The integrated peaks in the extracted profile reconvoluted with the smearing function (i.e., accuracy of the extracted data) were within 1% of the integrated peaks in the raw data where they were clearly resolved. Thus the extracted intensities are accurately represented to within ~1% (see Agard et al., 1981; Thomas and Agard, 1984). However, the deconvolution does not fit the observed data in the low resolution area very well, because of their different (radial) intensity profile shapes. The 1,1 and 2,0 reflections, which are near the beam stop are particularly sensitive and give the largest errors in fitting. Therefore, the 1,1 and 2,0 reflections were not used in data scaling, or to obtain Fourier difference maps.

Background Correction

A third source of error in reduced intensities is the background correction. This source of error is <1%, judged from comparisons of data deconvoluted from different films. A spline-fitted smooth background was removed from each pattern. To assess the effects of background removal on the intensities, slightly different backgrounds were removed from test patterns. The errors introduced were revealed as randomly distributed noise peaks rather than a pattern of peaks in the difference Fourier maps. Smoother background corrections resulted in less noise in the difference maps. In addition, the spline parameters were adjusted so as to not allow background curves that can reduce individual peaks. Curvature was so as to allow zeros, $dBg/ds = 0$, no closer than $\Delta S = 0.4$

Apportionment

Errors in the structure factors result from using the ratios of $F^2_{h,k}$ to $F^2_{k,h}$ from electron diffraction to derive the x-ray values that add to the observed total since these ratios for reflections will not be exactly the same for x-rays as for

TABLE I
STRUCTURE FACTORS FOR RECONSTITUTED $3Ca^{2+}$ NATIVE AND Pb^{2+}-LABELED PURPLE MEMBRANES

H	K	F_R	$F_{1Pb^{2+}}$	$F_{2Pb^{2+}}$	$F_{3Pb^{2+}}$
2	1	76 ± 1	74	69	68
1	2	127 ± 2	122	117	113
3	0	21 ± 1	21	25	24
2	2	102 ± 3	110	121	109
3	1	231 ± 3	217	204	213
1	3	74 ± 1	69	65	67
4	0	178 ± 2	173	174	168
3	2	121 ± 4	134	142	132
2	3	68 ± 2	76	81	76
4	1	207 ± 4	202	195	202
1	4	157 ± 3	153	147	153
5	0	212 ± 1	214	216	215
3	3	21 ± 1	21	24	24
4	2	68 ± 1	69	71	70
2	4	261 ± 1	265	273	271
5	1	31 ± 1	29	39	36
1	5	138 ± 4	129	176	165
6	0	31 ± 1	21	25	24
4	3	366 ± 6	369	367	379
3	4	200 ± 3	201	200	207
5	2	208 ± 3	240	225	230
2	5	72 ± 1	83	78	79
6	1	132 ± 6	146	150	136
1	6	35 ± 1	38	39	36
4	4	31 ± 1	21	25	25
7	0	96 ± 3	86	81	86
5	3	58 ± 2	51	48	51
3	5	193 ± 7	172	163	171
6	2	47 ± 1	39	45	36
2	6	51 ± 1	44	49	39
7	1	138 ± 3	134	134	126
1	7	180 ± 3	173	172	162

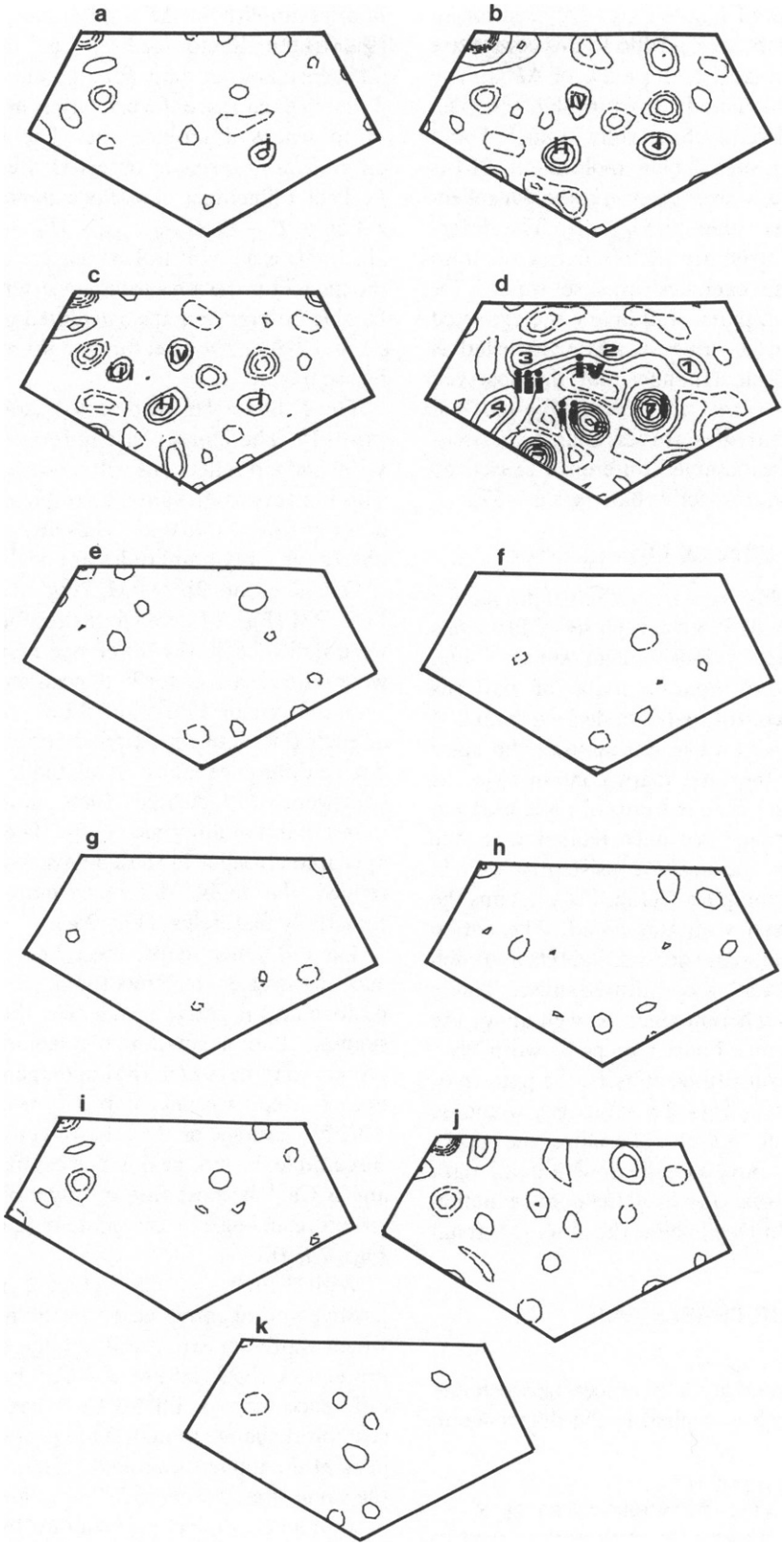

FIGURE 2 (*a*) Asymmetric unit of Fourier difference map of blue membranes containing 1 Pb^{2+}, minus blue membranes with Ca^{2+}. (*b*) Fourier difference map of 2 Pb^{2+} membranes. (*c*) Fourier difference map of 3 Pb^{2+} membranes. (*d*) Fourier map of reconstituted native PM, using $CaCl_2$. 1–7 mark the seven helices in a monomer of bR. i, ii, iii, and iv are the positions for the four refinable positive peak cation binding sites. Fourier difference maps were computed using observed difference amplitudes ($\Delta F = |F_{Pb}| - |F_R|$) and phase angles of native PM obtained by Hayward and Stroud (Hayward and Stroud, 1981). Observed amplitudes are shown in Table I. (*e*) Asymmetric unit of Fourier difference map between subsets containing 1 Pb^{2+}; (*f*) difference map between subsets containing 2 Pb^{2+}; (*g*) difference map between subsets containing 3 Pb^{2+}; (*h*) difference map between subsets of reconstituted native PM. Contour levels in the same as in *a–c*. (*i*) Asymmetric unit in a double difference map of 1 $Pb^{2+}|F_{Pb}| - |(F_R + f_p)|$ after refinement of 1 Pb^{2+} containing site, shown in *d* as *i*. (*j*) Double difference map of 2 Pb^{2+} membrane after refinement of sites i, ii, and iv shown in *d*; (*k*) double difference map of 3 Pb^{2+} membrane after refinement of sites i, ii, iii, and iv in *d*.

electrons. The same ratios of $I_{(hk)}$ to $I_{(kh)}$ were used for all patterns, hence if the errors in $|F^2_{hk}|$ due to this source are 2% of $|F^2_{hk}|$, the errors in ΔF^2_{hk} will be 2% of ΔF^2_{hk}. The average difference in calculated structure factors (i.e., $(||\Delta F|/|F||)$ upon addition of three fully occupied and perfectly ordered lead ion sites per bR molecule to PM is 15%. This is reduced due to overlap of *hk* and *kh* reflections to 10% signal in the value of $|F|_{(hk\,+\,kh)}$. The differences between observed structure factors extracted from one film vs. another, within each derivative set was 1% for the best, 5% for the worst pairs, well below the expected signal. However, the average values of $\Sigma\Delta F/\Sigma F_R$ listed as residuals (×100%) in Table II, show that the observed difference due to 3 Pb^{2+}-3 Ca^{2+} is ~8% of (F_R) (53% of theoretical), indicating that sites are less than fully occupied or fully ordered. The observed difference caused by addition of 1 Pb^{2+} between respective data sets is ~5%.

Observing the Effect of Overall Errors

To assess errors in amplitudes within each data set for reconstituted PM or for a derivative, each set of films was divided into two completely independent subsets. Fig. 2 *e–h* show the difference Fourier maps of patterns between subsets of the reconstituted data derived from 2–4 films each subset, and give an over-estimate of the noise level in the maps, since the final maps contain twice as many films in each data set. The patterns of noise peaks in these subset difference maps are uncorrelated with one another, and differ from the peaks consistently seen in maps from samples containing Pb^{2+} (Fig. 2 *a–c*). Thus the errors are small compared with the signal. The cation containing data sets were also divided into subsets and each subset was scaled to the 3 Ca^{2+} reconstituted subset. This is a further check that the coherent signal is well above the noise levels. In the difference Fourier maps between Pb^{2+} derivative and 3 Ca^{2+} reconstituted subsets, the pattern of peaks is the same as those in Figs. 2 *a–c* (as they would be exactly, if there were no noise). Therefore the peaks identified as cation sites are contained within all data subsets; the estimated errors caused by the data reduction of the bR x-ray patterns fall well below the observed signal upon addition of Pb^{2+}.

ERRORS IN THE PHASES AND REFINEMENT

Systematic errors due to phase differences between the phase for native bR, which is applied to the difference in Fourier amplitudes, $\Delta F = ||F_{Pb}| - |F_R||$, and the phase of f_p, (the structure factor for Pb^{2+}-Ca^{2+} in this case) occur in all difference Fourier maps for all molecular structures. These difference maps are the primary source of new information as to where differences lie. The interpretation of the differences in terms of observed sites results in phases for f_p. Thus refinement of site occupancies, based on minimization of $E = (\Sigma|F_{pb(hk\,+\,kh)}| - |F_R + f_p|_{(hk\,+\,kh)})^2$ (Katre et al., 1984) is a quantitative measure of the degree to which the model for the ion sites is consistent with the x-ray data. Double difference maps calculated using $\Delta\Delta F_{pb} = ||F_{pb}| - |F_R + f_p||$ then show features that are still unaccounted for by the model.

TABLE II
RESIDUALS CALCULATED BETWEEN DATA SETS

	*F*1	*F*2	*F*3
F_R	5.5%	8.4%	7.6%
F_1		5.3%	4.3%
F_2			4.4%

The *R* factor between scaled x-ray and em amplitudes was 0.19. Therefore, phase differences between the native x-ray and em reflections will be $\sim\sigma\phi \simeq 0.19$ radians = 11°. This is a very small value, corresponding to a drop in figure of merit from 1.0 to 0.98. Thus any errors due to use of em phases for x-ray amplitudes are negligible.

One site for Pb^{2+} PM (Fig. 2 *a*), three sites for 2 Pb^{2+}-PM (Fig. 2 *b*), and four sites for 3 Pb^{2+} PM (Fig. 2 *c*) were indicated in the difference maps, and all these sites were refined satisfactorily in position and occupancy.

In the case of 2 Pb^{2+} and 3 Pb^{2+} derivatives, refinement of each Pb^{2+} site was carried out independently, and the double difference maps calculated to ensure that the other sites were still indicated. Such maps are freer from noise than the initial difference maps. The other sites uniformly appeared stronger in these maps. With all the (four) sites refined, the double difference map 3 Pb^{2+} − 3 Ca^{2+} is essentially featureless (Fig. 2 *k*).

The difference maps, Figs. 2 *a*, *b*, *c* and double difference maps after refinement (Figs. 2 *i*, *j*) show alternating positive and negative peaks near the threefold axes. This suggests that a small rearrangement of either lipid or protein may have occurred upon generation of blue membranes, which was not completely restored upon addition of <3 Pb^{2+} cations, or that the threefold axis is particularly susceptible to error peaks. The comparison between 3 Pb^{2+} and 3 Ca^{2+} is most free of any stoichiometry dependent structure change in the protein (compare Fig. 2 *k* with Figs. 2 *i*, *j*).

With 2 Pb^{2+} − 3 Ca^{2+} (Fig. 2 *j*) there are additional positive and negative peaks in the double difference map which represent structural change in partially deionized protein, vs. the structure of 3 Ca^{2+}bR. Fig. 2 *i*, the double difference map for Pb^{2+}-3 Ca^{2+} has less apparent protein structural change though some peaks, such as the negative peak at the top left threefold axis, in the lipid region are at the same sites. Perhaps Ca^{2+} ions and not Pb^{2+} bind here, or movements in the lipid occur at this site, or the threefold axis has a higher multiplicity for the noise.

The phases used for generating the Fourier difference maps were the experimentally derived ones of Hayward and Stroud (1981). The expected change in the phases up to 7 Å due to the addition of Pb^{2+} is ~30° and is

progressively corrected during refinement of the Pb^{2+} sites as revealed in the improvement of the double difference maps (Fig. 2 *i–k*). The F_{000} term was derived from the ratio of protein to lipid of 1.3 in the native density map (Engelman et al., 1980). The refined occupancies for the sites are listed in Table III. The estimated errors in occupancy estimated as the sizes of shifts in parameters after convergence, were found to be 0.01–0.03 (Chambers and Stroud, 1979). Refined positions of the three sites present in both 2 Pb and 3 Pb were the same within ~1 Å, again indicating satisfactory refinement. The lower site occupancy of ~0.1 in 3 Pb^{2+} vs. 2 Pb^{2+} presumably arises from limitations in the refinement scheme, and gives an estimate of the overall errors in the refined parameters.

α-helices in bR, as seen in the electron density map of reconstituted native PM are numbered 1–7 in Fig. 2 *d*. The cation site of highest affinity is on helix 7. With a stoichiometry of two Pb^{2+} ions, a second site on helix 6 and a third between 2 and 3 appear. Addition of the third Pb^{2+} ion causes the membrane to regenerate completely to purple, with four sites, on helices 7, 6, close to helix 3 and between helix 2 and 3, respectively. These sites together account for 2.5 of the 3 available Pb^{2+} equivalents added to the membranes.

DISCUSSION

The relative affinity at each site is established in the 1 Pb^{2+}, 2 Pb^{2+}, 3 Pb^{2+} difference maps and the occupancies of the Pb^{2+} cations are similar at each site (0.47–0.95 Pb^{2+}) (Table III). The cation sites near helices 7, 6, 3, and 2/3 presumably bind to regions of negatively charged residues on the surface. The total refined occupancies of the Pb-Ca sites 0.6, 1.99, 2.50 in the 1 Pb^{2+}, 2 Pb^{2+}, 3 Pb^{2+} derivatives are fairly close to the stoichiometry of ions, therefore the binding sites are probably quite discrete. The cytoplasmic surface of PM is rich in carboxyl sidechains of residues, which could be candidates for cation binding. A negative surface potential is localized mainly on the cytoplasmic side (Ehrenberg and Berezin, 1984). Biochemical evidence suggests that at least one of the high affinity cation sites is on the COOH-terminal peptide sequence (Chang et al., 1985; Govindjee et al., 1984). Papain cleavage of PM that removes 17 of the COOH-terminal amino acids also diminishes the affinity of PM for cations and so generates blue membranes upon washing in distilled water, whereas native PM are stable in distilled water (our unpublished results; Chang et al., 1985). There are changes in the cation titration curves of these papain-treated membranes (Kimura et al., 1984). The occupancy at the first site (helix 7) is significantly less than at the second site. This may indicate that the cation associated near helix 7 may be more disordered and so contributes less to the diffraction; it may be involved with a mobile region of the protein, for example the COOH-terminus (Wallace and Henderson, 1982).

In their paper on location of the COOH-terminus of bR, Wallace and Henderson (1982) suggest that alternating positive and negative peaks in their Fourier difference maps may be due to rearrangement of either lipid or protein components in the membrane. Engelman and Zaccai (1980) in their work using deuterated valine and phenylalanine attribute the negative peaks in their difference maps to phase errors caused by the use of phases from native structure with amplitudes of the derivatives. Negative contours in difference Fourier maps of PM are expected in the light of the sources of error, but the refinement, possible in the case where discrete sites are located, its own self-consistency between different sets of observations, and a successful convergence we feel are essential to acceptance that given sites can account for all the peaks seen, both positive and negative.

It is noteworthy that a covalent heavy metal label (mercurilated phenylglyoxal) that we have located at Arg 225/227, where the chain leaves helix G to start the COOH-terminal peptide, shows a density peak on helix 6 in the Fourier difference maps (Katre et al., 1984), very close to site ii for divalent cations. Negatively charged binding sites for divalent cations on the cytoplasmic surface of PM could involve Asp 36/38 on the linking sequence between helices A–B and Asp 102/104 between helices C–D, as well as the COOH-terminal sequence (assignment of helices in Katre et al., 1984). Selective alteration of these negatively charged groups will pin down residues of the sequence involved in each cation binding site, and the location of these sequences in the tertiary structure of bacteriorhodopsin.

TABLE III
OCCUPANCY OF THE CATION BINDING SITES IN PURPLE MEMBRANES

Site	Location	Stoichiometric equivalents of Pb^{2+}/bR		
		1	2	3
(i)	helix 7	0.60*	0.68	0.52
(ii)	helix 6		0.78	0.95
(iv)	helix 2–3		0.53	0.47
(iii)	helix 3			0.55
Total occupancy		0.60	1.99	2.49

*Occupancy is given in lead ion equivalents. The errors in occupancy estimated from the sizes of shifts in parameters after convergence were ±0.01–0.03 (Chambers and Stroud, 1979). Occupancies of less than unity could be due to disorder of a fully occupied site, or to statistical occupation.

APPENDIX

The value of 12° was determined by simulating a Gaussian distribution of membrane misorientation, and calculating that value that would exactly duplicate the observed value of $n = 1.8$. However, a general idea of the misorientation required can be estimated as follows. The lowest resolution reflection used was the (2,1) reflection, of resolution 21 Å; the highest resolution reflection was the (7,1) of resolution 7.2 Å. Each reflection is extended in the Z direction by a distance at half height of $\sim 1/t$, where t is the thickness of the membrane, or ~45 Å. This follows since the transform

of a uniform leaflet of thickness t, perpendicular to the plane is $I(z^*) \sim (\sin(\pi ts)/(\pi ts))^2$. Thus half maximal intensity will lie at $S = \pm 0.44/t$ ($\simeq 1/2t$) = $\pm 1/102$ Å^{-1}. The second reflection, the (3,0) at a resolution of 18 Å resolution, would be diminished by misorientation of the membrane planes if some of the membranes were sufficiently misoriented that the falloff due to thickness (1/102) Å^{-1} placed them outside the equatorially sampled (3,0) reflection, i.e., if α, the misorientation angle, = 18/102 radians, or $\alpha \simeq \pm 10°$.

We thank Dr. J. Finer-Moore for invaluable assistance, Drs. R. H. Fairclough and Melvin O. Jones for discussion and assistance with recording the diffraction patterns. We are grateful to W. Stoeckenius who provided purple membranes, and for his encouragement.

Research was supported by the National Institutes of Health, grant (GM32079) to Robert M. Stroud.

Received for publication 23 September 1985 and in final form 11 February 1986.

REFERENCES

Agard, D. A., R. A. Steinberg, and R. M. Stroud. 1981. Quantitative analysis of electrophoretograms: a mathematical approach to super-resolution. *Anal. Biochem.* 111:257–268.

Bayley, H., K-S. Huang, R. Ramakrishnan, A. M. Ross, Y. Tagagaki, and H. G. Khorana. 1981. Site of attachment of retinal in bacteriorhodpsin. *Proc. Natl. Acad. Sci. USA.* 78:2225–2229.

Chambers, J. L., and R. M. Stroud. 1979. The accuracy of refined protein structures: comparison of two independently refined models of bovine trypsin. *Acta. Crystallogr. Sect. B.* 35:1861–1874.

Chang, C.-H., J.-G. Chen, R. Govindjee, and T. Ebrey. 1985. Cation binding by bacteriorhodopsin. *Proc. Natl. Acad. Sci. USA.* 82:396–400.

Dupuis, P., T. C. Corcoran, and M. A. El-Sayed. 1985. Importance of bound divalent cations to the tyrosine deprotonation during the photocycle of bacteriorhodopsin. *Proc. Natl. Acad. Sci. USA.* 82:3662–3664.

Ehrenberg, B., and Y. Berezin. 1984. Surface potential on purple membranes and its sidedness studied by a resonance Raman dye probe. *Biophys. J.* 45:663–670.

Engelman, D. M., R. Henderson, A. D. McLachlan, and B. A. Wallace. 1980. Path of the polypeptide in bacteriorhodopsin. *Proc. Natl. Acad. Sci. USA.* 77:2023–2027.

Engelman, D. M., and G. Zaccai. 1980. Bacteriorhodopsin is an inside-out protein. *Proc. Natl. Acad. Sci. USA.* 77:5894–5898.

Franks, A. 1955. An optically focusing x-ray diffraction camera. *Proc. Phys. Soc. Lond. Sect. B.* 68:1054–1064.

Govindjee, R., K. Kinosita, A. Ikegami, and T. Ebrey. 1980. Conformational changes of bacteriorhodopsin as probed by a fluorescent dye. *Biophys. J.* 45(2, Pt.2):214*a*. (Abstr.)

Hayward, S. B., and R. M. Stroud. 1981. Projected structure of purple membrane determined to 3.7 Å resolution by low temperature electron microscopy. *J. Mol. Biol.* 151:491–517.

Katre, N. V. 1984. Location of cation binding sites in the tertiary structure of purple membranes from halobacteria. International Symposium on Biomolecular Structure and Interactions. December 17–22, Bangalore, India.

Katre, N. V., J. Finer-Moore, S. Hayward, and R. M. Stroud. 1984. Location of an extrinsic label in the primary and tertiary structure of bacteriorhodopsin. *Biophys. J.* 46:195–204.

Katre, N. V., P. K. Wolber, W. Stoeckenius, and R. M. Stroud. 1981. Attachment site of retinal in bacteriorhodopsin. *Proc. Natl. Acad. Sci. USA.* 78:4068–4072.

Kimura, Y., A. Ikegami, and W. Stoeckenius. 1984. Salt and pH dependent changes of the purple membrane absorption spectrum. *Photochem. Photobiol.* 40:641–646.

Mathies, R., and L. Stryer. 1976. Retinal has a highly dipolar vertically excited singlet state: implications for vision. *Proc. Natl. Acad. Sci. USA.* 73:2169–2173.

Mowery, P. C., R. H. Lozier, Q. Chae, Y.-W. Tseng, M. Taylor, and W. Stoeckenius. 1979. Effect of acid pH on the absorption spectra and photoreactions of bacteriorhodopsin. *Biochemistry.* . 18:4100–4107.

Nakanishi, K., V. Balogh-Nair, M. Arnaboldi, K. Tsujimoto, and B. Honig. 1980. An external point-charge model for bacteriorhodopsin to account for its purple color. *J. Am. Chem. Soc.* 102:7945–7947.

Oesterhelt, D., and W. Stoeckenius. 1974. Isolation of the cell membrane of *Halobacterium halobium* and its fractionation into red and purple membrane. *Methods Enzymol.* 31:667–678.

Ross, M. J., M. W. Klymkowsky, D. A. Agard, and R. M. Stroud. 1977. Structural studies of a membrane-bound acetylcholine receptor from *Torpedo california. J. Mol. Biol.* 116:635–659.

Stoeckenius, W., and K. A. Bogomolni. 1982. Bacteriorhodopsin and related pigments of *Halobacteria. Annu. Rev. Biochem.* 51:587–616.

Thomas, G. J., and D. A. Agard. 1984. Quantitative analysis of nucleic acids, proteins and viruses by Raman band deconvolution. *Biophys. J.* 46:763–768.

Tsuji, K., and K. Rosenheck. 1979. The low pH species of bacteriorhodopsin. *FEBS (Fed. Eur. Biochem. Soc.) Lett.* 98:368–372.

Wallace, B. A., and R. Henderson. 1982. Location of the carboxyl terminus of bacteriorhodopsin in purple membrane. *Biophys. J.* 39:233–239.